Available online at www.sciencedirect.com
SCIENCE DIRECT®
International Journal of Heat and Mass Transfer 48 (2005) 1373–1383
International Journal of HEAT and MASS TRANSFER
www.elsevier.com/locate/ijhmt

Constructal multi-scale cylinders in cross-flow

T. Bello-Ochende, A. Bejan *

Department of Mechanical Engineering and Materials Science, Duke University, P.O. Box 90300, Durham, NC 27708-0300, USA

Received 6 April 2004; received in revised form 16 September 2004
Available online 15 December 2004

Abstract

This paper reports a new concept for maximizing heat transfer density in assemblies of cylinders in cross-flow: the use of cylinders of several sizes, and the optimal placement of each cylinder in the assembly. The heat transfer is by laminar forced convection with specified overall pressure difference. The resulting flow structure has multiple scales that are distributed nonuniformly through the available volume. Smaller cylinders are placed closer to the entrance to the assembly, in the wedge-shaped flow regions occupied by fluid that has not yet been used for heat transfer. The paper reports the optimized flow architectures and performance for structures with 1, 2 and 3 cylinder sizes, which correspond to structures with 1, 2 and 4 degrees of freedom. The heat transfer rate density increases (with diminishing returns) as the optimized structure becomes more complex. The optimized cylinder diameters are relatively robust, i.e., insensitive to changes in complexity and flow regime (pressure difference). The optimized spacings decrease monotonically as the driving pressure difference increases. The multi-scale flow architectures optimized in this paper have features and qualities similar to tree-shaped (dendritic) designs, where the length scales are numerous, hierarchically organized, and nonuniformly distributed through the available space.

Keywords: Constructal theory; Multi-scale; Cylinders in cross-flow; Forced convection; Animal design

1. Introduction

The maximization of the rate of heat transfer in a given space has been the driving force behind many of the miniaturization, augmentation and unconventional ways of designing structures for heat and fluid flow. The same trend is driven by the need to install more and more heat generating components into a given space. This activity has been described recently as a principle-based 'constructal' process [1] of generating flow architecture in the pursuit of global objective, subject to global constraints. The flow configuration is the unknown.

The constructal strategy is to endow the flow configuration with the freedom to change, and to search systematically for paths that lead to optimal or near-optimal flow configurations. Strategy and systematic search mean that architectural features that have been found beneficial in the past can be incorporated and compounded into more complex flow structures of the present. Strategy is important not only for accelerating the search in a design space that is infinite, but also for identifying the near-optimal designs that perform at nearly the same level as the absolute best. It is important to know the highest performance level and the frontiers of diminishing returns beyond which the search should be terminated. It is important to be reminded

* Corresponding author. Tel.: +1 919 660 5309; fax: +1 919 660 8963.
E-mail address: dalford@duke.edu (A. Bejan).

0017-9310/$ - see front matter © 2004 Elsevier Ltd. All rights reserved.
doi:10.1016/j.ijheatmasstransfer.2004.10.013

Nomenclature

Be	pressure drop number, Eq. (11)
D_0	diameter
k	thermal conductivity, W/mK
L_d	downstream flow length, m
L_u	upstream flow length, m
P	pressure, Pa
Pr	Prandtl number
q	total heat transfer, W
$\tilde{q}$	dimensionless heat transfer density, Eq. (12)
q''	heat transfer rate per unit length, W/m
q'''	heat transfer rate density, W/m^3
S_0	spacing between D_0 cylinders
T	temperature, K
T_w	wall temperature, K
T_0	inlet temperature, K
u, v	velocity components, m/s
x, y	cartesian coordinates, m

Greek symbols

α	thermal diffusivity, m^2/s
ΔP	pressure difference, Pa
θ	dimensionless temperature
μ	viscosity, kg/sm
ν	kinematic viscosity, m^2/s
ρ	density, kg/m^3
ϕ	porosity

Subscripts

m	maximized once
2m	maximized twice
3m	maximized three times
4m	maximized four times
opt	optimum
w	wall

Superscript

$(\sim)$	dimensionless variables, Eqs. (5 and 6)

that when the flow structure is complex, there are many winning structures on the podium of highest performance [2].

One class of heat and fluid flow structures that have been optimized in this spirit are the configurations in which optimal spacings exist: stacks of parallel plates, staggered plates, cylinders in cross-flow, and pin fin arrays with impinging flow. Optimal spacings have been determined for natural convection, and for forced convection with specified overall pressure difference. This work has been reviewed in Refs. [1] and [3], and is not reviewed again here. It has one important characteristic that links all the optimized configurations: the optimized spacing is a *single* length scale that is distributed *uniformly* throughout the given volume.

In this paper we propose to go beyond the single-spacing philosophy, and to explore the idea of optimizing flow structures with more than one free length scale. This direction of thought has a lot in common with the most recent work on tree-shaped flow structures [1–14], where the length scales are numerous, hierarchically organized and nonuniformly distributed through the available space. In the present paper, the multiple length scales are the diameters and spacings between cylinders in cross-flow. The largest cylinder diameter defines the overall extent of the flow space. The nonuniform distribution of these length scales means that progressively smaller cylinders are placed near the entrance to the assembly, i.e. in flow regions inhabited by fluid that has not participated in the global heat transfer enterprise.

2. Row of cylinders of one size

Consider the row of parallel cylinders shown in Fig. 1. The height of the assembly H and the cylinder diameter D_0 are fixed. The flow regime is driven by the pressure difference ΔP, which is maintained across the assembly. The first objective is to select the number of cylinders in the bundle, or the cylinder to cylinder spacing, S_0, such that the overall thermal conductance between the cylinder and the ambient air is maximal. The flow is assumed steady, laminar, incompressible and two-dimensional. All the thermophysical properties are assumed constant.

The lower part of Fig. 1 shows the elemental volume that characterizes this assembly. Symmetry allows us to study only half of the channel formed between two cylinders. The computational domain contains the flow region of length D_0, plus an upstream section $L_u \times \frac{1}{2}(D_0 + S_0)$, and a downstream section $L_d \times \frac{1}{2}(D_0 + S_0)$. The lengths L_u and L_d were selected based on accuracy tests described later in this section.

The conservation equations for mass, momentum and energy require

$$\frac{\partial u}{\partial x} + \frac{\partial v}{\partial y} = 0 \tag{1}$$

$$u\frac{\partial u}{\partial x} + v\frac{\partial u}{\partial y} = -\frac{1}{\rho}\frac{\partial P}{\partial x} + \nu\nabla^2 u \tag{2}$$

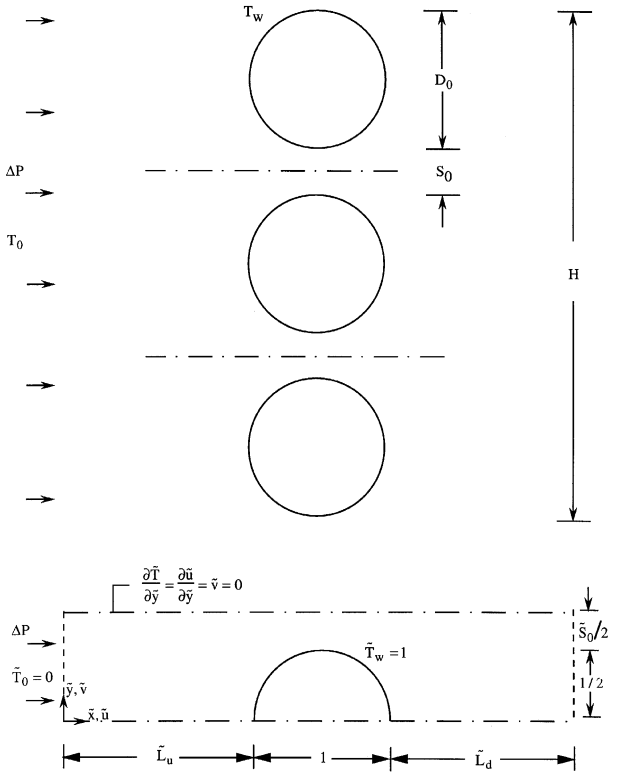

Fig. 1. Single row of cylinders in cross-flow, and the computational domain.

$$u\frac{\partial v}{\partial x}+v\frac{\partial v}{\partial y}=-\frac{1}{\rho}\frac{\partial P}{\partial y}+\nu\nabla^2 v \tag{3}$$

$$u\frac{\partial T}{\partial x}+v\frac{\partial T}{\partial y}=\alpha\nabla^2 T \tag{4}$$

where $\nabla^2 = \partial^2/\partial x^2 + \partial^2/\partial y^2$. The coordinate system (x, y) and velocity components (u, v) are defined in Fig. 1. The variables are defined in the Nomenclature. The work of solving Eqs. (1)–(4) numerically is based on a dimensionless formulation using the variables

$$(\tilde{x},\tilde{y})=\frac{(x,y)}{D_0}\quad(\tilde{u},\tilde{v})=\frac{(u,v)}{\Delta P D_0/\mu} \tag{5}$$

$$\widetilde{T}=\frac{T-T_\infty}{T_w-T_\infty}\quad P=\frac{\widetilde{P}}{\Delta P} \tag{6}$$

where T_w and T_∞ are the temperatures of the cylinder wall and the free stream. The resulting dimensionless equations are

$$\frac{\partial\tilde{u}}{\partial\tilde{x}}+\frac{\partial\tilde{v}}{\partial\tilde{y}}=0 \tag{7}$$

$$\frac{Be}{Pr}\left(\tilde{u}\frac{\partial\tilde{u}}{\partial\tilde{x}}+\tilde{v}\frac{\partial\tilde{u}}{\partial\tilde{y}}\right)=-\frac{\partial\widetilde{P}}{\partial\tilde{x}}+\nabla^2\tilde{u} \tag{8}$$

$$\frac{Be}{Pr}\left(\tilde{u}\frac{\partial\tilde{v}}{\partial\tilde{x}}+\tilde{v}\frac{\partial\tilde{v}}{\partial\tilde{y}}\right)=-\frac{\partial\widetilde{P}}{\partial\tilde{y}}+\nabla^2\tilde{v} \tag{9}$$

$$Be\left(\tilde{u}\frac{\partial\widetilde{T}}{\partial\tilde{x}}+\tilde{v}\frac{\partial\widetilde{T}}{\partial\tilde{y}}\right)=\nabla^2\widetilde{T} \tag{10}$$

where Pr is the Prandtl number ν/α, and Be is the dimensionless pressure drop number that Refs. [15,16] named the Bejan number,

$$Be=\frac{\Delta P D_0^2}{\alpha\mu} \tag{11}$$

The flow boundary conditions are indicated in the lower part of Fig. 1: no slip and no penetration on the plate surfaces; $\tilde{P}=1$, $\partial\tilde{u}/\partial\tilde{x}=\tilde{v}=0$ at the inlet of the computational plane; $\tilde{P}=0$ and $\partial(\tilde{u},\tilde{v})/\partial\tilde{x}=0$ at the exit of the computational domain; free slip and no penetration ($\partial\tilde{u}/\partial\tilde{x}=\tilde{v}=0$) on the horizontal surfaces of the upstream and downstream sections of the computational domain. The thermal boundary conditions are: $\widetilde{T}=1$ on the cylindrical surfaces, and $\widetilde{T}=0$ on the inlet plane of the computational domain. The remaining portions of the computational domain are adiabatic.

The spacing between cylinders varies. We are interested in the geometric arrangement that maximizes the

overall heat transfer between the cylinder and the surrounding fluids. The dimensionless quantity that is used to determine this quantity is the dimensionless heat transfer rate density. The heat transfer density rate is $q''' = q'/[D_0(D_0 + S_0)]$, where q' is the total heat transfer rate integrated over the surface of one cylinder. The corresponding q''' in the dimensionless form is

$$\tilde{q} = \frac{q'}{D_0(D_0 + S_0)k(T_w - T_0)} \tag{12}$$

Eqs. (8)–(10) were solved using a finite-element ode with four-node quadrilateral elements and linear interpolation functions [17]. The explicit appearance of the pressure in the momentum equation was eliminated by using the penalty function method. In all the simulations the compressibility parameter was fixed at 10^{-8}. For more details see Ref. [18]. The nonlinear equations resulting from the Galerkin finite-element discretization of Eqs. (8)–(10) were solved using successive substitution followed by a quasi-Newton method. The convergence criteria were

$$\frac{\|u^{(k)} - u^{(k-1)}\|}{\|u^k\|} \leqslant 10^{-4} \quad \text{and} \quad \frac{\|R(u^{(k)})\|}{\|R_0\|} \leqslant 10^{-4} \tag{13}$$

in which **R(u)** is the residual vector, **u** is the complete solution vector, k is the iteration counter, and $\|\cdot\|$ is the Euclidian norm. The grid was nonuniform in both $\tilde{x}$ and $\tilde{y}$ directions. The grid was double graded in the $\tilde{y}$ direction so as to put more nodes near the cylinder surfaces to capture more accurately the behavior in the boundary layers. The grid varied from one geometric configuration to another. Grid refinement tests performed in range ($10^3 \leqslant Be \leqslant 10^6$, $Pr = 0.72$) indicated that the solutions were insensitive to further grid doubling in $\tilde{x}$ and $\tilde{y}$ when 40 nodes per D_0 were used in both $\tilde{x}$ and $\tilde{y}$ directions. Table 1 shows how grid independence was achieved. Another set of accuracy tests showed that when $L_u/D_0 = 0.8$ and $L_d/D_0 = 1.6$, the channel heat transfer rate varied less than 1% after the doubling of the upstream and downstream lengths. Based on these tests, the numerical results discussed in this paper we obtained with grids of 40 nodes per D_0, and with $\tilde{L}_u = 0.8$ and $\tilde{L}_d = 1.6$.

Table 1
Grid refinement tests for $\tilde{S}_0 = 0.3$, $Be = 10^3$, $Pr = 0.72$, for calculation of $\tilde{q}$

Number of nodes per D_0 in the $\tilde{x}$ and $\tilde{y}$ directions	$\tilde{q}$	$\left\lvert\frac{\tilde{q}^i - \tilde{q}^{i+1}}{\tilde{q}^i}\right\rvert$
10	6.376	–
20	6.482	0.0167
40	6.529	0.0073
80	6.544	0.0023

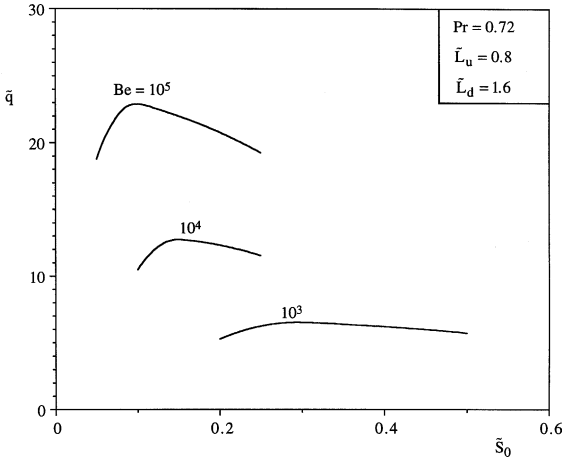

Fig. 2. The maximization of heat transfer density in the assembly of Fig. 1.

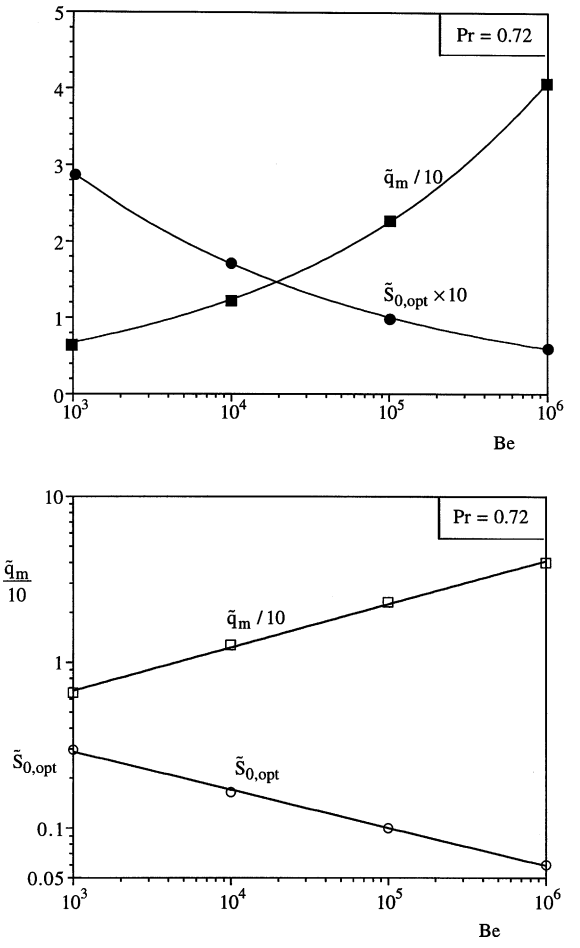

Fig. 3. The optimal spacing and maximal heat transfer density for the row of cylinders shown in Fig. 1.

3. Optimal spacing

The flow and temperature fields were simulated in a large number of configurations, in order to determine the effect of spacing on heat transfer density. Fig. 2 shows that the heat transfer density is maximal when S_0 has an optimal value, which decreases as the pressure drop number Be increases. The optimal spacings determined in this manner are summarized in Fig. 3, in linear and logarithmic form. The later shows that for $Pr = 0.72$ they are correlated within 0.15% by the power law

$$\frac{S_{0,\mathrm{opt}}}{D_0} = 1.41Be^{-0.23} \tag{14}$$

The corresponding heat transfer density maxima are also reported in Fig. 3. They are correlated within 0.1% by the expression

$$\tilde{q}_{\mathrm{m}} = 1.1Be^{0.26} \tag{15}$$

These results are in agreement with the constructal method (Ref. [1], Chapter 3), according to which maximal heat transfer density means 'optimal packing' such that flow regions that do not contribute to global performance are eliminated. This means that optimal packing in Fig. 1 is achieved when the cylinders are brought close enough so that their thermal boundary layers just touch. The thermal boundary layer of a cylinder with laminar flow and $Pr > 1$ has a thickness of order

$$\delta_T \sim D_0 Re^{-1/2} Pr^{-1/3} \tag{16}$$

The velocity scale V that appears in the Reynolds number $Re = VD_0/\nu$ is determined from the longitudinal force balance on the control volume that contains a single cylinder,

$$\Delta P S_0 \sim F \tag{17}$$

where F is the drag force,

$$F \sim \tau D_0 S_0 \tag{18}$$

where the shear stress scale is $\tau \sim \mu V/S_0$. Combining Eqs. (17) and (18) we find

$$Re \sim \frac{Be^{2/3}}{Pr^{8/9}} \tag{19}$$

The range $10 < Re < 10^3$ corresponds to the range $10^3 < Be < 10^6$ used in this paper. By Setting $\delta_T \sim S_0$ in Eq. (16) and using Eq. (19), we find that

$$\tilde{S}_0 \sim Be^{-1/3} Pr^{-1/9} \tag{20}$$

which for $Pr \sim 1$ anticipates very well the numerical correlation (14).

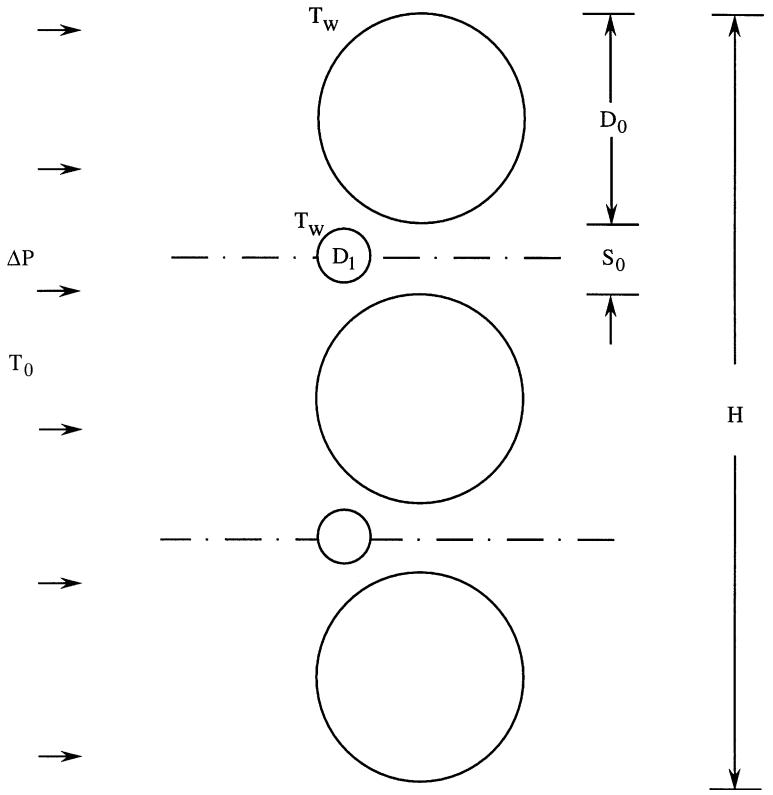

Fig. 4. Row of cylinders with two sizes (two degrees of freedom).

The heat transfer rate density (15) can be anticipated based on the same scaling argument. The cylinder heat flux scale is $q'' \sim k(T_w - T_0)/\delta_T$, where $\delta_T \sim S_0 \sim D_0\tilde{S}_0$. Because $S_0 < D_0$, cf. Eq. (20) for $Be \gg 1$, the heat transfer rate density is $q''' \sim q''/D_0$, such that the dimensionless heat transfer rate density becomes

$$\tilde{q} \sim \frac{q'''D_0^2}{k(T_w - T_0)} \sim Be^{1/3}Pr^{1/9} \tag{21}$$

This prediction agrees very well with the numerical correlation (15) when $Pr \sim 1$.

4. Cylinders with two sizes

In the second phase of this study we considered the more complex structure shown in Fig. 4. Cylinders of smaller diameter (D_1) were inserted in the entrance (converging) regions of the channels formed between the original cylinders. This structural change brings with it one more degree of freedom: the small-cylinder diameter $\tilde{D}_1 = D_0/D_1$. The flow configuration has two degrees of freedom, which are represented by $\tilde{D}_1$ and the original spacing $\tilde{S}_0$.

The numerical procedure for flow simulation and geometry optimization was the same as the procedure tested in Section 2. As shown in the example of Fig. 5, the pressure drop number Be was fixed, and many configurations ($\tilde{D}_1$, $\tilde{S}_0$) were simulated in search for the configuration with the highest heat transfer density $\tilde{q}$. This procedure was then repeated over the range $10^3 \leqslant Be \leqslant 10^6$ and $Pr = 0.72$.

The results are condensed in linear and logarithmic form in Fig. 6, which shows how the optimized configuration and the maximized performance vary with the pressure drop number. The optimal small diameter is independent of Be: the optimal ratio D_1/D_0 is practically constant and equal to 0.25. The optimal spacing decreases as Be increases. This behavior is consistent with what we saw in Fig. 3, however the $\tilde{S}_{0,opt}$ values of Fig. 6 are consistently larger than the optimal spacings reported in Fig. 3. The optimal spacing is larger when a smaller cylinder is placed in the mouth of the channel. The data of Figs. 3 and 6 show that the ratio of the optimized spacings is practically independent of Be,

$$\frac{\tilde{S}_{0,opt}(\text{Fig. 6})}{\tilde{S}_{0,opt}(\text{Fig. 3})} \cong 1.75 \tag{22}$$

The maximized heat transfer density shown in Fig. 6 increases with Be. This trend is qualitatively in agreement with the results obtained for single-scale structures (Fig. 3), however, in Fig. 6 the effect of Be is stronger. The subscript 2m is a reminder that $\tilde{q}$ was maximized with respect to two geometric parameters, $\tilde{S}_0$ and $\tilde{D}_1$.

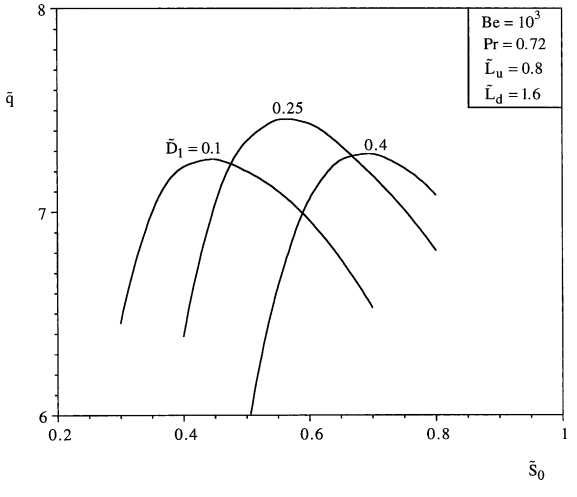

Fig. 5. The maximization of heat transfer density in the assembly of Fig. 4.

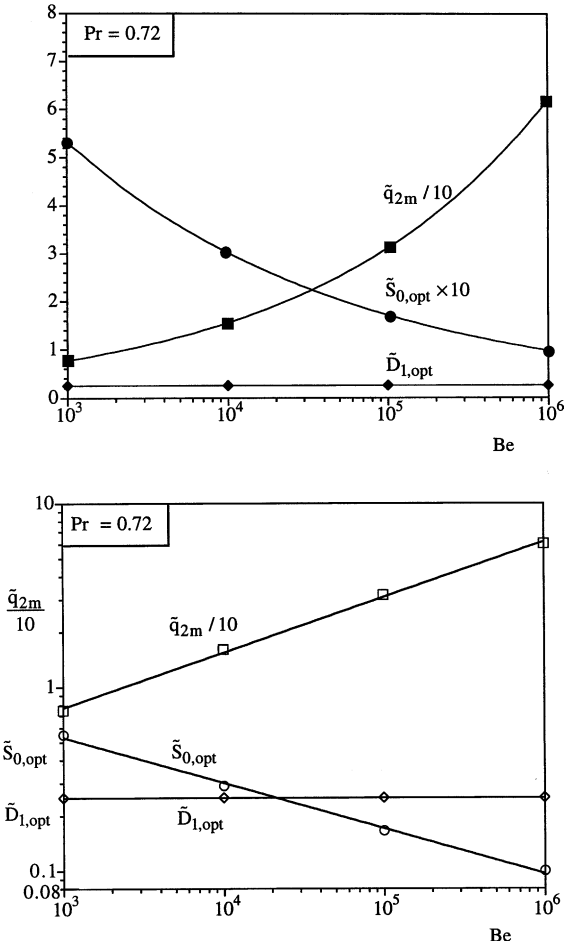

Fig. 6. The optimal spacing, optimal diameter ratio $\tilde{D}_1$ and maximal heat transfer density for the assembly shown in Fig. 4.

In place of Eq. (15), the $\tilde{q}_{2m}$ data of Fig. 6 are correlated within 0.06% by the power law $\tilde{q}_{2m} = 0.96Be^{0.3}$. It can be verified that $\tilde{q}_{2m}$ (Fig. 6) $> \tilde{q}_m$ (Fig. 3), which means that the use of two scales (D_0, D_1) brings about an increase in heat transfer rate density. We return to this observation in the discussion of Fig. 12.

5. Cylinders with three sizes

In the next step of this sequence of refining the flow structure, we inserted even smaller cylinders (D_2) in the entrance regions formed between the D_0 and D_1 cylinders. This new configuration is shown in Fig. 7. It has four degrees of freedom, $\widetilde{S}_0$, $\widetilde{D}_1$, $\widetilde{D}_2$ and the new spacing $\widetilde{S}_2$, which is the new center-to-center spacing between the D_1 and D_2 cylinders. The numerical procedure was the same as in the simulations and optimizations described in Sections 3 and 4. One difference was that the number of nodes per length scale D_0 was increased to 80, to capture well the development of the boundary layer around the smallest cylinder.

The search for the optimal flow configuration was conducted at fixed *Pr* and *Be*, and was organized in a sequence for nested optimization loops. The innermost loop (level I) is illustrated in Fig. 8, where three of the geometric parameters were fixed ($\widetilde{S}_0$,$\widetilde{D}_1$, $\widetilde{D}_2$), and the fourth ($\widetilde{S}_2$) was optimized such that $\tilde{q}$ reached its maximum value, $\tilde{q}_m$.

At level II, the procedure of level I was repeated for several values of $\widetilde{D}_2$ until the family of calculated $\tilde{q}$ maxima revealed a maximum value with respect to having varied $\widetilde{S}_2$ and $\widetilde{D}_2$. This second level is illustrated by the constant-$\widetilde{D}_2$ curves shown in Fig. 8.

The optimization results obtained at the end of levels I and II are summarized in Fig. 9, where the notation $\tilde{q}_{2m}$ is a reminder that the reported heat transfer density was maximized with respect to two geometric parameters, $\widetilde{S}_2$ and $\widetilde{D}_2$. Fig. 9 shows that $\tilde{q}_{2m}$ can be maximized with respect to the third free parameter, $\widetilde{S}_0$. This optimization constitutes level III, and its chief result—the heat transfer density maximum $\tilde{q}_{3m}$—is reported in Fig. 10.

Level IV is the maximization of $\tilde{q}_{3m}$ with respect to fourth free parameter, $\widetilde{D}_1$. Fig. 10 shows that $\tilde{q}_{3m}$ reaches a maximum at a distinct $\widetilde{D}_1$ value, which completes the description of the optimal flow configuration for the specified *Be* and *Pr* values. These final results are reported in Fig. 11, which summarizes the rest and

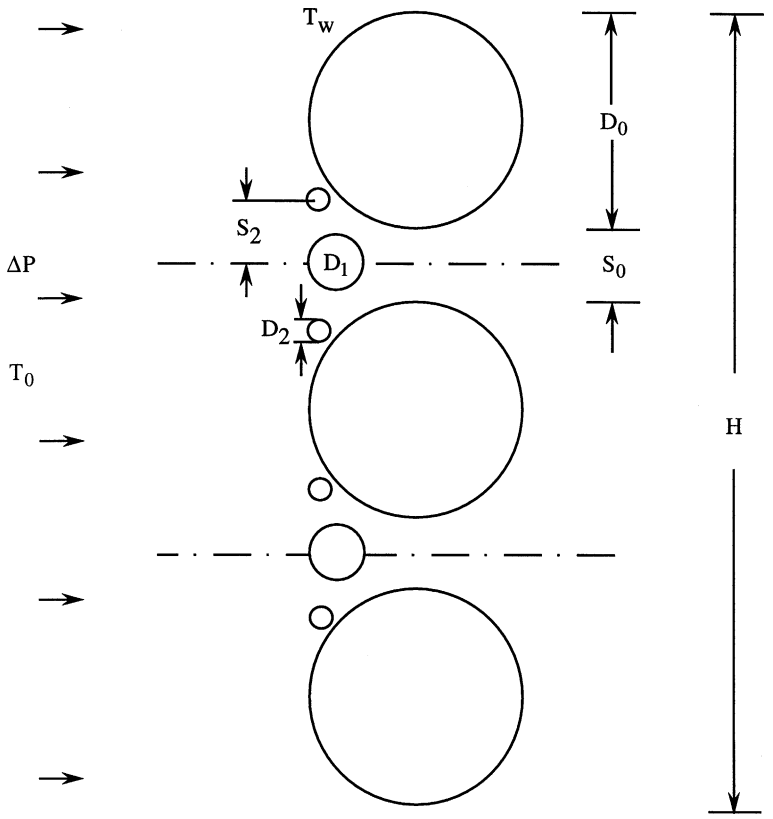

Fig. 7. Row of cylinders with three sizes (four degrees of freedom).

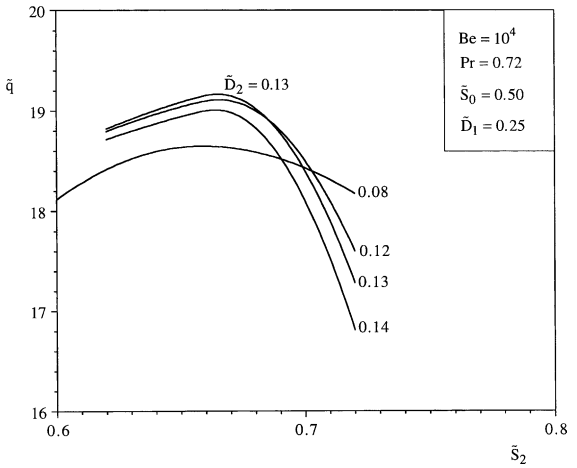

Fig. 8. The maximization of heat transfer density with respect to $\widetilde{S}_2$ and $\widetilde{D}_2$ in the configuration of Fig. 7.

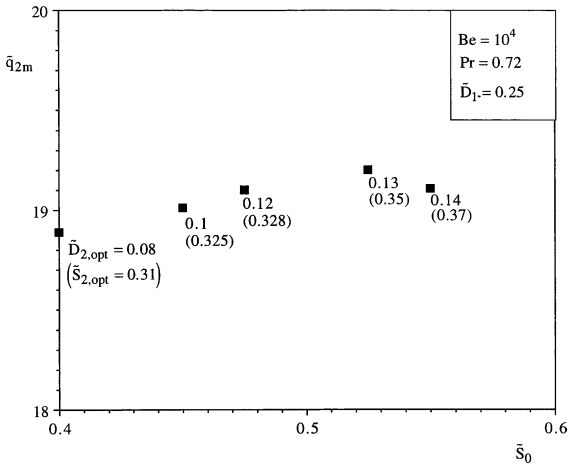

Fig. 9. The maximization of heat transfer density with respect to $\widetilde{S}_2$, $\widetilde{D}_2$ and $\widetilde{S}_0$ in the configuration of Fig. 7.

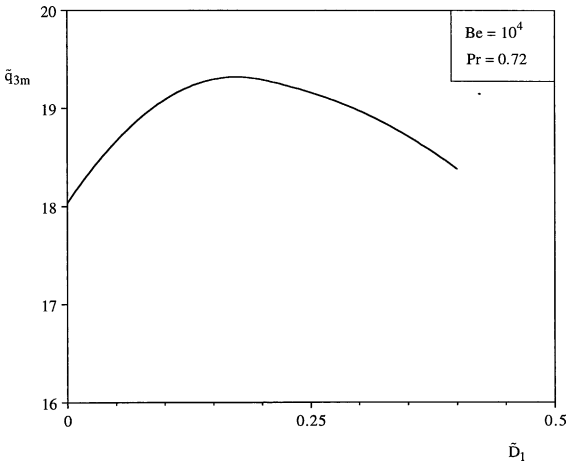

Fig. 10. The maximization of heat transfer density with respect to $\widetilde{S}_2$, $\widetilde{S}_0$, $\widetilde{D}_2$ and $\widetilde{D}_1$ in the configuration of Fig. 7.

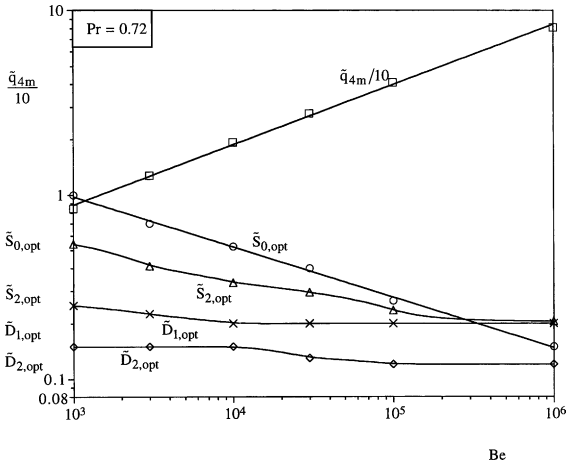

Fig. 11. The optimal spacings and diameters, and the maximal heat transfer density for the assembly shown in Fig. 7.

most voluminous part of the numerical work: the repeat of the 4-level optimization for several *Be* values in the range $10^3 \leqslant Be \leqslant 10^6$.

The trends revealed by Fig. 11 are similar to what we saw in Fig. 6, however, the differences are both interesting and important. One difference is that when a new cylinder is placed in the space between two older cylinders, the optimized spacing between the older cylinders increases to accommodate the new cylinder. More exactly, the $\widetilde{S}_{0,\mathrm{opt}}$ spacing increases by the factor

$$\frac{\widetilde{S}_{0,\mathrm{opt}}(\text{Fig. 11})}{\widetilde{S}_{0,\mathrm{opt}}(\text{Fig. 6})} \cong 1.68 \tag{23}$$

which is practically independent of *Be*. Another important change is that the maximized heat transfer rate density, which is correlated by $\tilde{q}_{4\mathrm{m}} \cong 0.91 Be^{0.33}$, is larger than all the heat transfer rate densities calculated previously. This finding is summarized in Fig. 12, which shows that the maximized heat transfer rate density increases as the number of geometric degrees of freedom increases. Fig. 12 also shows that diminishing returns (smaller $\tilde{q}$ increases) are registered as the flow configuration acquires more length scales. Although in accordance with constructal theory the optimization of complexity is beneficial, the cost of design and construction puts an end to the multi-scale optimization sequence.

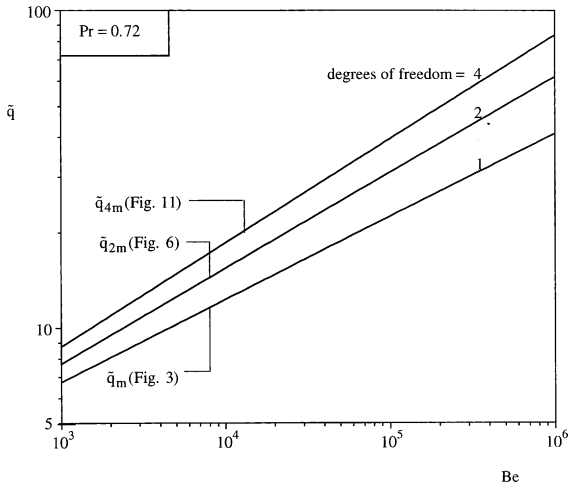

Fig. 12. Diminishing returns: the effect of the increasing complexity on the maximum heat transfer rate density.

6. Conclusions

In this paper we illustrated a new approach to the conceptual design of convective structures with maximal heat transfer density: the use of multiple length scales that are distributed nonuniformly through the available volume. For illustration, we used parallel cylinders in cross-flow forced convection. We installed new cylinders with progressively smaller diameters in the entrance wedges between older cylinders, where the flow regions were inhabited by fluid that had not been used for heat transfer.

Three classes of configurations were optimized and reported: cylinders with one, two and three sizes, which resided in flow structures with one, two and four degrees of freedom. The maximized heat transfer density increases from one class to the next, however, diminishing returns are noticed when the number of degrees of freedom increases from two to four. The optimized cylinder diameters are robust, i.e., relatively insensitive to changes in the number of scales and the flow regime (*Be*).

In Fig. 13(a) and (b), we drew to scale the optimized flow architectures with one, two and four freely varying length scales, cf. Figs. 1, 4 and 7, respectively. Read from left to right, the figure shows how the spacing between older cylinders increases when new cylinders are placed in the existing gaps. Read from Fig. 13(a) and (b), the montage shows that when the flow becomes faster the spacings become noticeably smaller, while the cylinder diameters do not change much. This last observation is relevant not only in heat exchanger design but also in animal design. A morphing multi-scale structure is robust when it can perform optimally under different flow conditions (slow, fast) by using the same solid parts. It is a lot easier for the structure to adapt itself by optimizing its fluid spacings, as opposed to redesigning its solid components. One example from the animal realm is the multi-channel organization of a swarm of bees [19]. The solid components (the bees) are permanent features, while the airways change with the inlet temperature of the ambient air that cools the swarm (see also Ref. [1], pp. 44–45).

Another way to summarize the evolution of the optimized flow architecture as the number of scales and the

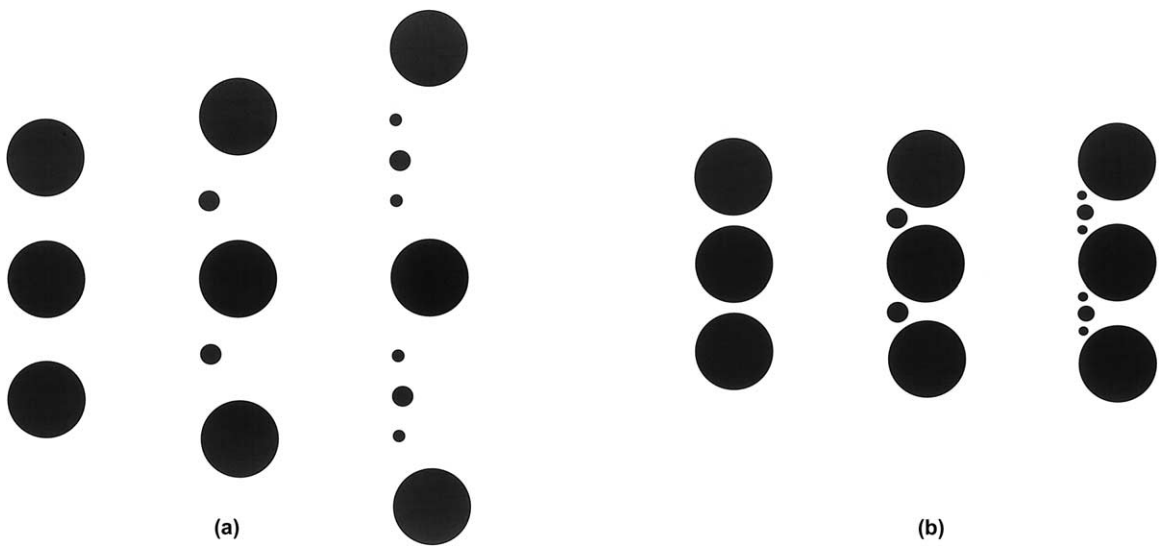

Fig. 13. The effect of increasing complexity and pressure drop number (*Be*) on the optimized multi-scale structure: (a) $Be = 10^3$; (b) $Be = 10^6$.

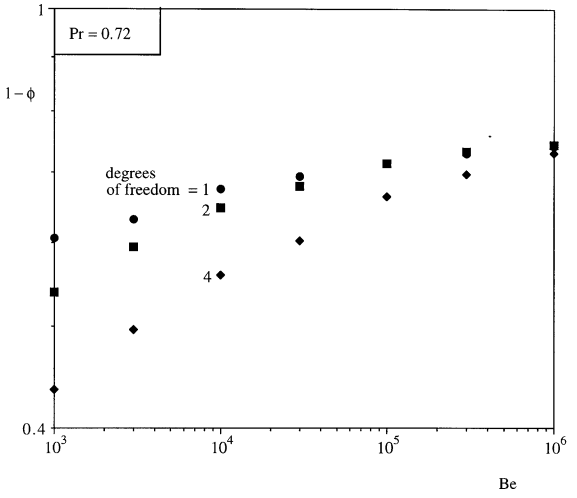

Fig. 14. The solidity of the optimized multi-scale structure.

pressure drop change, is to monitor the changes in the use of solid (cylinder) material. In each of Figs. 1, 4 and 7, the available flow space is a rectangle of size $D_0 \times \phi H$, where H is much greater than D_0. Both H and D_0 are fixed. The relative amount of cylinder material is expressed by the solidity of the assembly, $1-\phi$, where ϕ is the porosity: ϕ = (fluid space)/D_0H. Fig. 14 shows that the solidity of the optimized structure decreases as the number of degrees of freedom increases, and as Be decreases. This global indicator of the use of solid material suggests another way of reporting the global heat transfer performance of the optimized structures. Instead of the total heat transfer rate installed in the available volume, $\tilde{q}$, we may report the total heat transfer rate associated with the installed solid. This new measure is proportional to $\tilde{q}(1-\phi)$, which is shown now in Fig. 15. As in Fig. 12, performance increases as

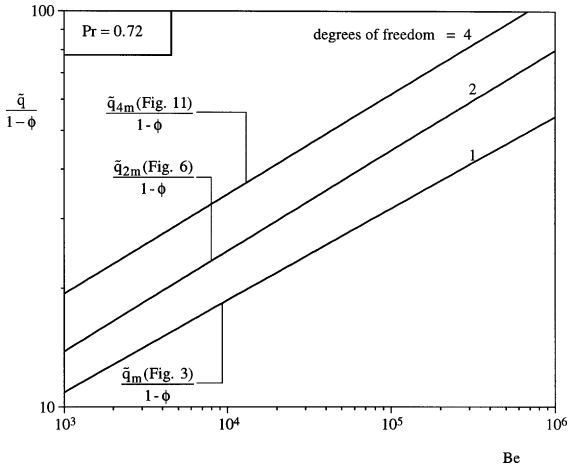

Fig. 15. The maximized heat transfer rate per unit of solid volume.

the number of degrees of freedom of the optimized structure increases, however, diminishing returns are not as evident as in Fig. 12. In conclusion, if we account for the use of solid material, the concept of multi-scale cylinders in cross-flow is even more promising.

In this paper we considered only the laminar range of the multi-scale cylinders optimization problem. We have every reason to expect that the design concept proposed in this paper can also be used when the flow is turbulent. This extension deserves to be explored in future research.

References

[1] A. Bejan, Shape and Structure, from Engineering to Nature, Cambridge University Press, Cambridge, UK, 2000.

[2] A. Bejan, S. Lorente, The constructal law and the thermodynamics of flow systems with configuration, Int. J. Heat Mass Transfer 47 (2004) 3203–3214.

[3] A. Bejan, I. Dincer, S. Lorente, A.F. Miguel, A.H. Reis, Porous and Complex Flow Structures in Modern Technologies, Springer-Verlag, New York, 2004.

[4] D.V. Pence, Reduced pumping power and wall temperature in microchannel heat sinks with fractal-like branching channel networks, Microscale Thermophys. Eng. 6 (2002) 319–330.

[5] Y. Chen, P. Cheng, Heat transfer and pressure drop in fractal tree-like microchannel nets, Int. J. Heat Mass Transfer 45 (2002) 2643–2648.

[6] Z.-Z. Xia, Z.-X. Li, Z.-Y. Guo, Heat conduction optimization: high conductivity constructs based on the principle of biological evolution, 12th International Heat Transfer Conference, Grenoble, France, 18–23 August 2002.

[7] D. Tondeur, L. Luo, U. D'Ortona, Optimisation des transferts et des materiaux par l'approche constructale, Entropie 30 (2000) 32–37.

[8] M.-O. Coppens, Y. Cheng, C.M. van den Bleek, Controlling fluidized bed operation using a novel hierarchical gas injection system, Paper 304d, AIChE Annual Meeting, Dallas, TX, 31 October–5 November 1999.

[9] H. Brod, Residence time optimised choice of tube diameters and slit heights in distribution systems for non-Newtonian liquids, J. Non-Newtonian Fluid Mech. 111 (2003) 107–125.

[10] T. Borrvall, A. Klarbring, J. Petersson, B. Torstenfelt, Topology optimization in fluid mechanics, in: H.A. Mang, F.G. Rammerstorfer, J. Eberhardsteiner (Eds.), Proccedings of the 5th WCCM V, World Congress on Computational mechanics, Vienna, 7–12 July 2002.

[11] J. Lewins, Bejan's constructal theory of equal potential distribution, Int. J. Heat Mass Transfer 46 (2003) 1541–1543.

[12] H. Poirier, Une théorie explique l'intelligence de la nature, Sci. Vie 1034 (2003) 44–63.

[13] A. Bejan, Y. Fautrelle, Constructal multi-scale structure for maximal heat transfer density, Acta Mech. 163 (2003) 39–49.

[14] R.N. Rosa, A.H. Reis, A.F. Miguel (Eds.), Bejan's constructal theory of shape and structure, Évora Geophysics Center, University of Évora, Portugal, 2004.
[15] S. Bhattacharjee, W.L. Grosshandler, The formation of wall jet near a high temperature wall under microgravity environment, ASME HTD 96 (1988) 711–716.
[16] S. Petrescu, Comments on the optimal spacing of parallel plates cooled by forced convection, Int. J. Heat Mass Transfer 37 (1994) 1283.
[17] FIDAP Theory Manual, Fluid Dynamics International, Evanston, IL, Revision 8.6, 1998.
[18] J.N. Reddy, D.K. Gartling, The Finite Element Method in Heat Transfer and Fluid Dynamics, CRC Press, Boca Raton, Florida, 1994.
[19] B. Heinrich, The mechanisms and energetics of honeybee swarm temperature regulation, J. Exp. Biol. 91 (1981) 25–55.